Fundamental Research 4 (2024) 868–881

Contents lists available at ScienceDirect

Fundamental Research

journal homepage: http://www.keaipublishing.com/en/journals/fundamental-research/

Article

A primary battery for efficient cadmium contamination remediation and electricity generation

Chaowen Chen[a,d], Jia Zhang[a,d,*], Guilong Zhang[c], Dongfang Wang[b], Jun Wang[a,d], Dongqing Cai[b,*], Zhengyan Wu[a,d,*]

[a] Key Laboratory of High Magnetic Field and Ion Beam Physical Biology, Hefei Institutes of Physical Science, Chinese Academy of Sciences, Hefei 230031, China
[b] College of Environmental Science and Engineering, Donghua University, Shanghai 201620, China
[c] School of Pharmacy, Binzhou Medical University, Yanta 264003, China
[d] Key Laboratory of Environmental Toxicology and Pollution Control Technology of Anhui Province, Hefei Institutes of Physical Science, Chinese Academy of Sciences, Hefei 230031, China

ARTICLE INFO

Article history:
Received 18 October 2022
Received in revised form 9 December 2022
Accepted 6 March 2023
Available online 25 March 2023

Keywords:
Primary battery
Electrolyte
KCl
Cd^{2+} removal
Electricity production

ABSTRACT

In this work, two kinds of primary batteries, both of which included a Zn anode, C rod cathode, copper wire and electrolyte composed of Cd^{2+}-contaminated water or soil, were constructed in the first attempt to both remove Cd^{2+} and generate electricity. Unlike traditional technologies such as electrokinetic remediation with high energy consumption, this technology could realize Cd^{2+} migration to aggregation and solidification and generate energy at the same time through simultaneous galvanic reactions. The passive surface of Zn and C was proven via electrochemical measurements to be porous to maintain the relatively active galvanic reactions for continuous Cd^{2+} precipitation. Cd^{2+} RE (removal efficiency) and electricity generation were investigated under different conditions, based on which two empirical models were established to predict them successfully. In soil, KCl was added to desorb Cd^{2+} from soil colloids to promote Cd^{2+} removal. These systems were also proven to remove Cd^{2+} efficiently when their effects on plants, zebrafish, and the soil bacterial community were tested. LEDs could be lit for days by utilizing the electricity produced herein. This work provides a novel, green, and low-cost route to remediate Cd^{2+} contamination and generate electricity simultaneously, which is of extensive practical significance in the environmental and energy fields.

1. Introduction

Pollution by heavy metal ions, especially Cd^{2+}, has become an important environmental issue worldwide [1–3]. Many toxic Cd^{2+} ions can be discharged into water and soil by a wide range of industries, including electronics, alloy manufacturing, mining, and refining [4]. Owing to its high solubility and migration, Cd^{2+} tends to be widely contaminated and enter the human body through the food chain [5]. Exposure to Cd^{2+}, even at a very minute concentration, can increase the possibility of human cancer and teratogenesis of the kidney, lung, liver, and reproductive organs [6,7]. Moreover, Cd^{2+} possesses the characteristics of persistence, nonbiodegradability, and bioaccumulation, so its toxicity can last for a long time. Therefore, remediation of Cd^{2+}-contaminated water and soil is of great significance.

In the past few decades, a variety of conventional methods have been developed to remove Cd^{2+} from the environment, such as precipitation [8–10], ion exchange [11–13], adsorption [14–16], reverse osmosis [17], evaporation recovery [18], and electrokinetic remediation [19,20]. These technologies can remove Cd^{2+} to different extents; nevertheless, they have some disadvantages. Precipitation, ion exchange and adsorption are ineffective at low Cd^{2+} concentrations [18], restricting their large-scale application. Reverse osmosis and evaporation recovery possess relatively high costs and may produce toxic substances [18,21,22]. Electrokinetic remediation generally exhibits high energy consumption and complex operation [23]. For electrokinetic treatment in both water and soil, electrolysis can introduce H^+ and OH^- at the anode and cathode, respectively, resulting in a substantial pH change [24]. For soil, a chelate such as ethylene diamine tetraacetic acid, which may be used to desorb Cd^{2+} on the soil surface, has low biodegradability [24]. These disadvantages greatly restrict the wide application of conventional methods in Cd^{2+} removal. Therefore, developing an economical and environmentally friendly approach to efficiently remove Cd^{2+} from the environment is urgently needed.

Abbreviations: CWBPB, Cd^{2+}-contaminated water based primary battery; CSBPB, Cd^{2+}-contaminated soil based primary battery; RE, removal efficiency.

* Corresponding authors.
E-mail addresses: zhangj@iim.ac.cn (J. Zhang), dqcai@dhu.edu.cn (D. Cai), zywu@ipp.ac.cn (Z. Wu).

https://doi.org/10.1016/j.fmre.2023.03.001

Until now, primary battery systems have been widely used in the energy generation field owing to the advantages of low cost and easy manufacturing [25–27]; they work by deriving electrical energy from spontaneous redox reactions within the battery. Generally, a primary battery consists of an anode, cathode, and electrolyte containing ions such as Zn^{2+} and NH_4^+ [28–30]. We hypothesized that if Cd^{2+}-contaminated water or soil was used as an electrolyte, the Cd^{2+} therein may be removed through electric field force and precipitation via galvanic reactions. Importantly, the system could generate electricity at the same time and show little influence on media pH without water electrolysis.

Herein, we developed a novel primary battery consisting of a Zn anode, C cathode, copper wire, and the electrolyte composed of Cd^{2+}-contaminated water or soil. The influence of environmental factors on Cd^{2+} RE and output current in water was investigated. Two empirical models were established to reveal the relationship among them. In soil, a certain amount of KCl was added for Cd^{2+} desorption from the soil colloid surface, enhancing Cd^{2+} RE. To elucidate the mechanism, the interactions among the Zn anode, C cathode, and electrolyte were studied via elementary, XRD, XPS, and electrochemical analyses. The promoting effects of this technology on plants, zebrafish, and soil bacterial communities were investigated to evaluate its applicability. This work provides an economical and green approach to remove Cd^{2+} and generate electricity simultaneously.

2. Materials and methods

2.1. Materials

Zn sheet (60 mm × 35 mm × 2 mm), C rods (diameter: length = 8 mm: 200 mm, 12 mm: 200 mm, 14 mm: 60 mm, 16 mm: 350 mm, and 20 mm: 200 mm), cuboid tanks (80 mm × 50 mm × 80 mm, 300 mm × 180 mm × 200 mm), LEDs (5 mm, emitting wavelengths of 645 and 467 nm), and copper wires were provided by Jinming Educational Instrument Co. (Jiangsu, China). $Cd(NO_3)_2{\cdot}4H_2O$, KCl, HCl and other chemicals of analytical reagent grade were purchased from Sinopharm Chemical Reagent Company (Shanghai, China). Water spinach was purchased from a supermarket on Dongpu Island (Hefei, China). Adult zebrafish (Danio rerio of both sexes) with a mean mass of 0.52 g was provided by China Zebrafish Resource Center. *N. benthamiana* seedlings (20 d after sprouting, length of 3 cm) and *Arabidopsis* seedlings (14 d after sprouting, length of 3 cm) were purchased from Miaoling biotechnology Co. Ltd. (Wuhan, China). Soil and sand (20–50 mesh) were taken from Dongpu Island (Hefei, China). Deionized water was used in all the experiments except pot experiments and fish tests.

2.2. Construction of a Cd^{2+}-contaminated water based primary battery (CWBPB) for removal of Cd^{2+}

$Cd(NO_3)_2{\cdot}4H_2O$ with given amounts were dissolved in 150 mL of deionized water to obtain Cd^{2+} aqueous solutions with a given concentration (50, 100, 200, 400 and 800 mg/L). Then the resulting aqueous solution with a given pH (5.5, 6.5, 7.5 and 8.5) was added to a tank (80 mm × 50 mm × 80 mm) at a certain temperature (20, 30 and 40 ˚C). Zn sheet and C rod (diameter of 8, 12, 14, 16 and 20 mm) with a given spacing (2, 4 and 6 cm) were inserted parallel in the middle of the tank with immersion depth of 2.4 cm. Subsequently, the Zn anode and C cathode were connected together with a copper wire (length of 40 cm, diameter of 1 mm) to obtain the CWBPB. After different intervals, the resulting solution was stirred (120 rpm) for 1 min and then 1 mL of the solution was taken out to measure Cd^{2+}concentration. After that, the RE of Cd^{2+} was calculated according to the following equation:

$$RE(\%) = \left(C_0 - C_t\right)/C_0 \times 100\%$$

where C_0 and C_t (mg/L) are the initial and residual concentrations of Cd^{2+}. Additionally, the influence of coexisting ion (SO_4^{2-} and Cl^-) on Cd^{2+} RE was investigated.

2.3. Electrochemical analyses

To be consistent with the application conditions of Cd^{2+} removal, Zn sheet and C rod (diameter of 14 mm) were prepared at its pristine form without treatment. 150 mL of Cd^{2+}-contaminated aqueous solution with concentration of 100 mg/L was added into a tank (80 mm × 50 mm × 80 mm), used as the electrolyte and the saturated calomel (SCE) was served as a reference electrode. For voltametric study of Zn, Zn sheet acted as a working electrode and C rod served as a counter electrode. While for voltametric study of C, the opposite is the case. The voltametric study included OCP and polarization curves at given intervals (1 h, 1 d, 3 d and 5 d) were conducted in a CHI-660E electrochemical workstation.

EIS spectra of Zn in the electrolyte for 1 h, 1 d, 3 d and 5 d were also investigated using a CHI-660E electrochemical workstation. The amplitude of applied potential was 10 mV and the frequency range analyzed was 0.01 Hz to 100 kHz. The experimental data was fitted using the equivalent circuit simulation program ZsimpWin.

2.4. Construction of a CSBPB for removal of Cd^{2+} and Cd

Dry soil (50–100 mesh) was evenly mixed with dry sand (20–50 mesh) at a weight ratio of 3:7. $Cd(NO_3)_2{\cdot}4H_2O$ (20.6, 41.2, 206, 412 and 824 mg) and KCl (0, 37.3, 74.6, 186.4 and 372.8 mg) were evenly mixed with soil-sand of given amount to obtain 150 g of mixture. After that, deionized water with a given volume (7.9, 26.5 and 50 mL) was evenly added to the system to obtain Cd^{2+}-contaminated soil. Then the resulting soil with a given pH (5.2, 4.8 and 4.4) was placed in a tank (80 mm × 50 mm × 80 mm and 300 mm × 180 mm × 200 mm) at a certain temperature (5, 20 and 40 ˚C). Zn sheet and C rod (diameter of 8, 12, 14, 16 and 20 mm) with a spacing of 4 cm were inserted parallel in the tank with immersion depth of 2.4 cm. Afterward, the Zn anode and C cathode were connected with a copper wire (length of 40 cm, diameter of 1 mm) to obtain the CSBPB. After 120 h, 5 g of the resulting soil from the middle part of the tank was taken out and put in 25 mL of 0.1 mol/L $CaCl_2$ aqueous solution. The resulting system was shaken (160 rpm) for 2 h at 20 ˚C. Then, the resulting suspension was centrifuged at 4,800 rpm for 5 min, and the Cd^{2+}concentration in the supernatant was measured. The RE of Cd^{2+} was can be calculated.

To determine the concentration of total Cd, another 0.2 g of the resulting soil was taken out from different locations in the tank and put in 10 mL of aqua regia. The resulting system was kept steadily for 72 h and then centrifuged at 4,800 rpm for 5 min. After that, the Cd concentration in the supernatant was measured to calculate the Cd RE.

2.5. Effect of K^+ on Cd^{2+} leaching in a soil-sand column

A certain amount of dry soil-sand mixture (with weight ratio of 3:7) were prepared to construct 4 different soil-sand columns: (I) 3 g of soil-sand was mixed evenly with KCl (with K^+ weight of 74.55 mg), and the resulting mixture was placed in a polyvinyl chloride tube (cylindrical, diameter of 2 cm, height of 10 cm); (II) 3 g of soil-sand without treatment was placed in that tube; (III) the mixture of soil-sand (3 g), Cd^{2+} (6 mg), and K^+ (74.55 mg) was placed in the tube; (IV) the mixture of soil-sand (3 g) and K^+ (74.55 mg) was placed in the tube. Subsequently, 15 mL of Cd(II)-contaminated water (50 ppm) was added on (I) and (II), and deionized water was added on (III) and (IV) to collect the leachate, respectively. After 24 h, the content of Cd^{2+} and K^+ in the leachate was measured.

2.6. Water spinaches pot experiments

Water spinaches (length of 5–10 cm, diameter of approximately 1 cm) with certain amount were cultivated in plastic pots (trapezoidal shape, height of 6.5 cm, width of 7.8 cm (bottom) and 11.3 cm (top), and length of 13.4 cm (bottom) and 17.2 cm (top)). The pots contained

the mixture of 450 mL of tap water and 50 mL of Cd^{2+} aqueous solution after treatment with CWBPB (C_0 = 50 mg/L, 20 °C, pH = 6.5, tank size of 80 mm × 50 mm × 80 mm, electrode spacing of 6 cm, and C rod diameter of 14 mm) for 0, 1 and 5 d respectively. The pot with 500 mL of tap water was set as the control. The systems were placed in a greenhouse (30 °C, humidity of 30%) for 7 d. The plant height, root length, chlorophyll content in leaves and Cd content in water spinaches were measured.

2.7. N. benthamiana and Arabidopsis pot experiments

As for *N. benthamiana*, 75 g of Cd^{2+} (37.5 mg/kg)-contaminated soil after treatment with CSBPB (moisture of 25%, pH = 5.2, 20 °C, KCl amount of 372.8 mg, tank size of 80 mm × 50 mm × 80 mm, C rod diameter of 14 mm, electrode spacing of 4 cm) for 0 and 5 d was evenly mixed with 175 g of soil-sand mixture. As for *Arabidopsis*, 50 g of Cd^{2+} (37.5 mg/kg)-contaminated soil after treatment with the same CSBPB for 0 and 5 d was evenly mixed with 200 g of soil-sand mixture. Then the resulting system was placed in a circular pot with height of 6 cm, diameters of 7 cm (top) and 6.5 cm (bottom), respectively. After that, *N. benthamiana* and *Arabidopsis* with certain amounts were planted in the pots respectively. The systems were placed in a greenhouse (25 °C, humidity of 30%) for 20 d. Finally, the plant height, root length, biomass, and Cd content of these two plants were measured.

2.8. Effect of CWBPB treatment on zebrafish

Six zebrafish were placed in a tank (8 cm × 5 cm × 8 cm) containing 200 mL of tap water or Cd^{2+}- contaminated water after treatment with CSBPB (C_0 = 12 mg/L, 20 °C, pH = 6.5, tank size of 80 mm × 50 mm × 80 mm, electrode spacing of 6 cm, and C rod diameter of 14 mm) for 0 and 5 d, respectively. After 2 d, the zebrafish viability was calculated via counting the number of zebrafish alive. Additionally, the expression levels of 5 genes in zebrafish were analyzed using qRT-PCR.

2.9. Electricity generation from primary battery

Cd^{2+}-contaminated water (80 mL, 800 mg/L) or soil-sand mixture (80 g, 800 mg/kg) was added to a bottle. A Zn sheet (cylindrical, 157 mm × 60 mm) was placed in a plastic bottle (cylindrical, diameter of 5 cm and height of 8 cm) along the inner surface. Then a C rod (diameter of 14 mm) was inserted in the middle of the bottle with immersion depth of 5 cm. Afterward, four bottles were connected in series to form a primary battery, wherein the Zn sheet of one bottle was connected to the C rod in the next bottle with a copper wire (length of 10 cm, diameter of 1 mm). Subsequently, the primary battery, a multimeter and a certain number of LEDs were connected in series to form a circuit. After certain intervals, the emission spectrum of LEDs was measured. Meanwhile, the current and voltage of the circuit were measured to calculate the output power.

2.10. Characterization

The morphologies and elemental mapping of precipitates were observed by a scanning electron microscope (SEM) (Sirion 200, FEI Co., USA) with an energy dispersive X-ray spectroscope (EDX). The structure and chemical states analyses were conducted on a TTR-III X-ray diffractometer (XRD) (Rigaku Co., Japan) and an X-ray photoelectron spectroscope (XPS) (ESCALAB 250, Thermo-VG Scientific Co., USA). Cd^{2+} concentration was measured using an inductively coupled plasma-optical emission spectrometer (ICAP7200, Thermo Fisher Scientific, USA). The current and voltage were determined using a multimeter (VC 97, Victor Co., China).

3. Results and discussion

3.1. Structure and mechanism of the primary battery

To remove Cd^{2+} and generate electricity simultaneously, two kinds of primary batteries, namely, CWBPB and CSBPB, were constructed using Cd^{2+}-contaminated water and soil as the electrolyte, respectively. The structure and mechanism of these two primary batteries are shown in Fig. 1a and 1b, respectively. CWBPB consisted of a Zn sheet (anode), a C rod (cathode), Cd^{2+}-contaminated water (electrolyte), and a copper wire. Therein, the Zn anode and C cathode were connected with the copper wire. Galvanic reactions in CWBPB can be divided into anodic and cathodic parts. The anodic reactions involve the spontaneous dissolution and passivation of Zn to form Zn^{2+} and ZnO [31,32], as shown in reactions (1) and (2), respectively. The generation of ZnO is attributed to the migration of OH^- from the C rod to Zn forced via the derived electric field, resulting from the redox of dissolved O_2 [31] at the cathode through the electrons donated by Zn (reaction (3)). Subsequently, Cd^{2+} in water migrates toward the cathode under the electric field, which could react with OH^- to give $Cd(OH)_2$ precipitate on the C rod surface and in the water bottom (reaction (4)). As a result, Cd^{2+} could be efficiently removed from water when the C rod was removed or the solution was filtered. Notably, spontaneous galvanic reactions in the electrolyte result in electricity production, which could be conveniently applied, such as to power LED lights.

$$\text{anode: } Zn - 2e^- = Zn^{2+} \ (\varphi^{\theta}_{Zn(II)/Zn} = -0.7618\ V) \quad (1)$$

$$Zn + 2OH^- - 2e^- = ZnO + H_2O \ (\varphi^{\theta}_{Zn(II)/Zn} = -1.249\ V) \quad (2)$$

$$\text{cathode: } O_2 + 2H_2O + 4e^- = 4OH^- \ (\varphi^{\theta}_{O(0)/O(-II)} = 0.401\ V) \quad (3)$$

$$Cd^{2+} + 2OH^- = Cd(OH)_2 \quad (4)$$

For CSBPB, the structure and mechanism are similar to those of CWBPB. Herein, Cd^{2+} tends to be adsorbed by negatively charged soil

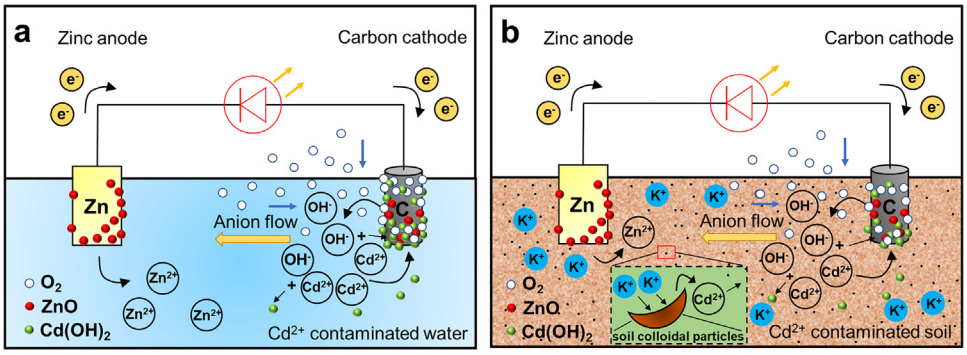

Fig. 1. Mechanism of primary battery based on Cd^{2+}-contaminated (a) water and (b) soil.

colloidal particles, which greatly limits Cd^{2+} migration. This is unfavorable for Cd^{2+} removal and electricity generation. To solve this problem, KCl, which is capable of enhancing soil fertility [33], was added to the soil to desorb Cd^{2+} from soil colloidal particles through ion exchange (rectangular inset of Fig. 1b). Similar to that in water, a $Cd(OH)_2$ precipitate is formed in the soil around the C cathode, and thus, the soil could be removed to realize Cd^{2+} removal. It can also be learned from reactions (2) and (4) that the generated OH^- can react with Zn^{2+} and Cd^{2+}, resulting in a relatively stable pH in this system. As a result, this technology may impose little impact on the surroundings compared with traditional electrokinetic remediation.

3.2. Removal performance of the primary battery for Cd^{2+} in water

The RE of CWBPB on Cd^{2+} in water was investigated. Fig. 2a shows that after 4 d, the RE of Cd^{2+} decreased from 92.5% to 22.6% as the Cd^{2+} initial concentration increased (C_0) from 50 to 800 mg/L. As shown in Fig. 2b, Cd^{2+} RE increased with increasing pH from 5.5 to 8.5, likely because high pH could facilitate the formation of $Cd(OH)_2$ precipitates via reaction (4). Considering the convenience of application, 6.5 was selected as the optimal pH. As illustrated in Fig. 2c, with increasing temperature, RE increased slowly because reaction (4) was slightly accelerated at higher temperatures. Meanwhile, the influence of coexisting ions, including Cl^- (NaCl) and SO_4^{2-} (Na_2SO_4), on the removal performance of CWBPB for Cd^{2+} was investigated. Fig. 2d shows that they could increase Cd^{2+}RE significantly, particularly for SO_4^{2-}. This was because both Cl^- and SO_4^{2-} could increase the electric conductivity of the electrolyte, wherein SO_4^{2-}, with more charges, showed a higher effect than Cl^-. Therefore, Cl^- and especially SO_4^{2-} greatly accelerated the migration of Cd^{2+} in the electrolyte and electrons in copper wires, promoted the galvanic reactions and formation of $Cd(OH)_2$ around the C rod, and thus increased Cd^{2+}RE. As a result, they both, especially SO_4^{2-}, could effectively increase output currents (Fig. S1a).

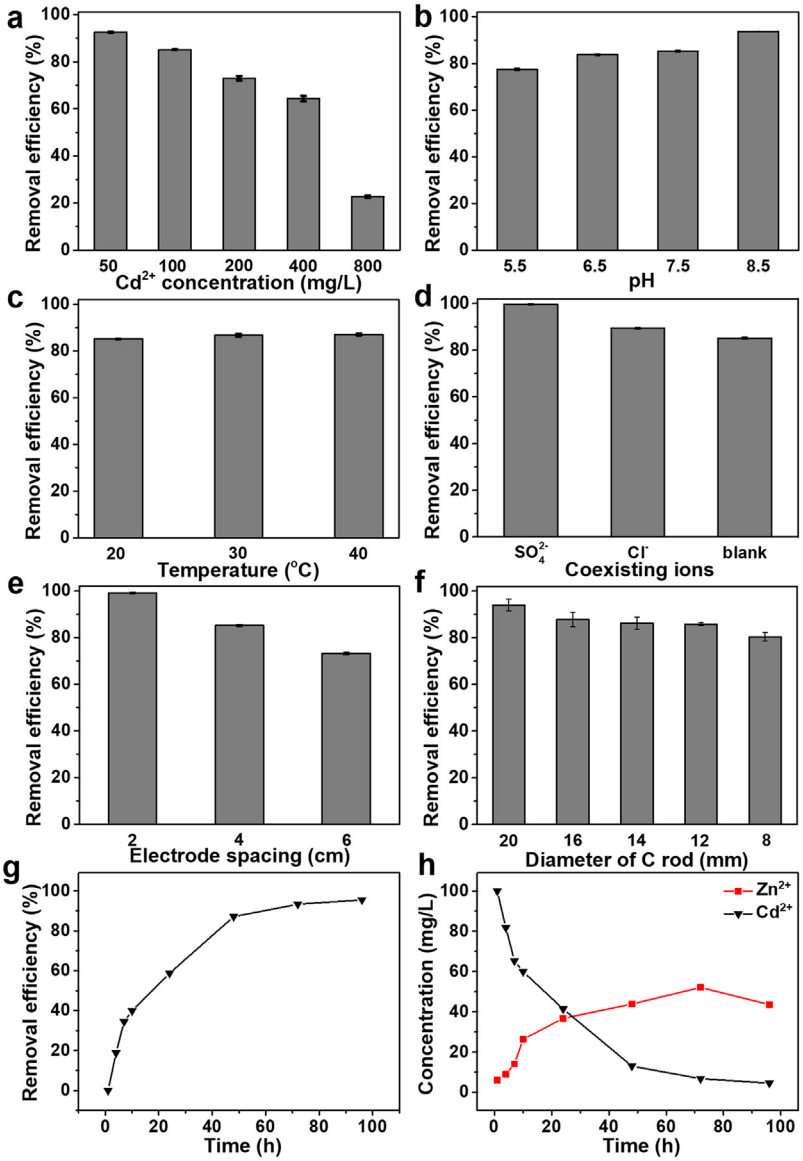

Fig. 2. Effects of (a) C_0 on RE of Cd^{2+} (pH = 6.5, 20 °C), (b) pH on RE of Cd^{2+} (C_0 = 100 mg/L, 20 °C), (c) temperature on RE of Cd^{2+} (C_0 = 100 mg/L, pH = 6.5), (d) coexisting SO_4^{2-} and Cl^- (200 mg/L) on RE of Cd^{2+} (C_0 = 100 mg/L, pH = 6.5, 20 °C) from aqueous solution by CWBPB (tank size of 80 mm × 50 mm × 80 mm, electrode spacing of 4 cm, C rod diameter of 14 mm) for 4 d; Effects of (e) electrode spacing (C rod diameter of 14 mm) and (f) C rod diameter (electrode spacing of 4 cm) on RE of Cd^{2+} (C_0 = 100 mg/L, 20 °C, pH = 6.5, tank size of 80 mm × 50 mm × 80 mm) from aqueous solution by CWBPB for 4 d; (g) Cd^{2+} RE and (h) Cd^{2+} and Zn^{2+}concentrations with time in aqueous solution treated by CWBPB (C_0 = 50 mg/L, 20 °C, pH = 6.5, tank size of 80 mm × 50 mm × 80 mm, electrode spacing of 4 cm, and C rod diameter of 14 mm).

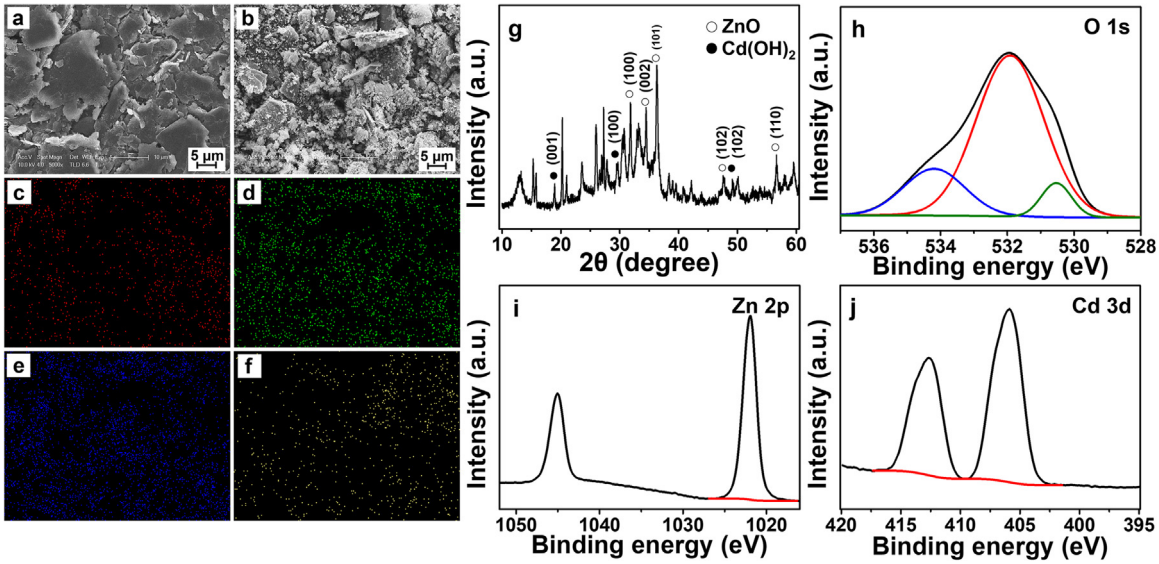

Fig. 3. SEM images of C rod surface (a) before and (b) after CWBPB treatment, (c-f) distribution maps of C, O, Zn and Cd on C rod surface, and (g) XRD and XPS (h-j: O 1s, Zn 2p, Cd 3d) spectra of precipitates on C rod after CWBPB treatment for 4 d (C_0 = 50 mg/L, 20 °C, pH = 6.5, tank size of 80 mm × 50 mm × 80 mm, electrode spacing of 4 cm and C rod diameter of 14 mm).

Additionally, the influence of the electrode spacing and diameter of the C rod on the Cd^{2+} RE was studied. As the electrode spacing increased, the electrolyte possessed a lower conductivity, resulting in a lower current, as shown in Fig. S1b. In that case, the migration of Cd^{2+}-ions in the electrolyte and electrons in the copper wire was inhibited, which was unfavorable for reactions (1–4) and resulted in a lower Cd^{2+}-RE (Fig. 2e). As illustrated in Fig. 2f, Cd^{2+} RE decreased from 94.0% to 80.4% as the C rod diameter decreased from 20 to 8 mm. This was because the C rod with a larger diameter possessed a higher conductivity, promoting the migration of electrons and Cd^{2+} and thus reactions (1–4).

The removal performance of CWBPB on Cd^{2+} in water over time was investigated. As displayed in Fig. 2g, the RE of Cd^{2+} increased rapidly within the initial 48 h and slowly afterward, and thus, the Cd^{2+} concentration decreased correspondingly (Fig. 2h). In addition, the concentration of Zn^{2+} increased slowly within the initial 72 h because of the oxidation of the Zn anode, as shown in Eq. 1. Interestingly, the Zn^{2+}concentration decreased afterward, likely because some Zn^{2+} reacted with OH^- to obtain ZnO via reaction (5) [31]

$$Zn^{2+} + 2OH^- = ZnO + H_2O \quad (5)$$

The reuse performance of primary batteries in water has been investigated. To maintain the reactivity of the anode and cathode, both the Zn sheet and C rod were polished using emery papers (500 mesh) before reuse. As shown in Fig. S2, the removal efficiency of Cd^{2+} in 96 h does not decrease after three cycles, even though the output current remains stable. These results imply that the primary battery can be used to remove Cd^{2+} at least 3 times.

Additionally, the morphologies of the C rod surfaces before and after CWBPB treatment were observed. The raw C rod consisted of abundant micro flakes with a smooth surface (Fig. 3a). After Cd^{2+} removal for 4 d, plenty of micronano particles appeared and were distributed evenly on the C rod surface (Fig. 3b). Moreover, Zn, Cd and O were found in the EDX spectrum of the C rod (Fig. S3) and distributed uniformly on the C rod surface (Fig. 3c-f), confirming that the micro/nanoparticles mainly consisted of these three elements.

XRD measurements were carried out to study the crystal structure and components of the micro/nanoparticles on the C rod. Fig. 3g shows that characteristic peaks of $Cd(OH)_2$ (18.9° (001), 29.5° (001), and 49.0° (102)) and ZnO (31.8° (100), 34.4° (002), 36.3° (101), 47.5° (102), and 56.6° (110)) were found in the XRD spectrum, which well matched the standard JCPDS card (No. 31–0228 and No. 36–1451). This result indicated that the micronano particles were mainly composed of $Cd(OH)_2$ and ZnO, which were generated via reactions (4) and (5), respectively. Additionally, the XRD peaks proved that $Cd(OH)_2$ and ZnO possessed crystal structures, which could also be confirmed by the TEM images in Fig. S4.

XPS analysis was conducted to further investigate the chemical states of the particles. The O 1s peak in Fig. 3h could be deconvoluted into three peaks at 530.5, 531.9 and 534.1 eV, ascribed to O atoms in ZnO, $Cd(OH)_2$ and –OH, respectively [34–36]. In addition, the Zn $2p_{3/2}$ peak at 1,021.9 eV in Fig. 3i was attributed to ZnO. For Cd 3d (Fig. 3j), the $3d_{3/2}$ and $3d_{5/2}$ peaks at 406 and 412.7 eV were ascribed to $Cd(OH)_2$. This result demonstrated that the particles mainly consisted of $Cd(OH)_2$ and ZnO, which was consistent with the XRD result.

Based on the preceding analyses, CWBPB exhibited outstanding removal performance for Cd^{2+}. Importantly, after Cd^{2+} removal, only a small amount of Zn^{2+} remained in the water because most Zn^{2+} was transformed to ZnO via reaction (5). In other words, this technology did not introduce secondary pollution, displaying its environmental friendliness.

3.3. Electrochemical investigation

To further demonstrate the mechanism of Cd^{2+} removal via the primary battery, electrochemical measurements were conducted on CWBPB, which covered the galvanic reactions and precipitation processes. Fig. 4a and 4b describe the open circuit potential (OCP) curves of the anode (Zn sheet) and cathode (C rod) during immersion in Cd^{2+} solution (100 ppm) for 30 min, respectively. Remarkably, the Cd^{2+} solution applied in the OCP investigation was initially prepared without aeration to simulate the practical conditions during Cd^{2+} removal, except when specifically mentioned. In Fig. 4a, the OCP of Zn shifts gradually toward the anodic direction with an increment of approximately only 45 mV in 30 min, which may be attributed to the slight formation of a passive layer. As illustrated in reactions (2) and (5), the migrated OH^- from the cathode may assist in forming ZnO. The passivation of zinc in Cd^{2+} solution can be consolidated according to the obtained results. For the C rod in Cd^{2+} solution, the OCP exhibits a relatively fast variation toward the cathodic direction (Fig. 4b), which can contribute to the for-

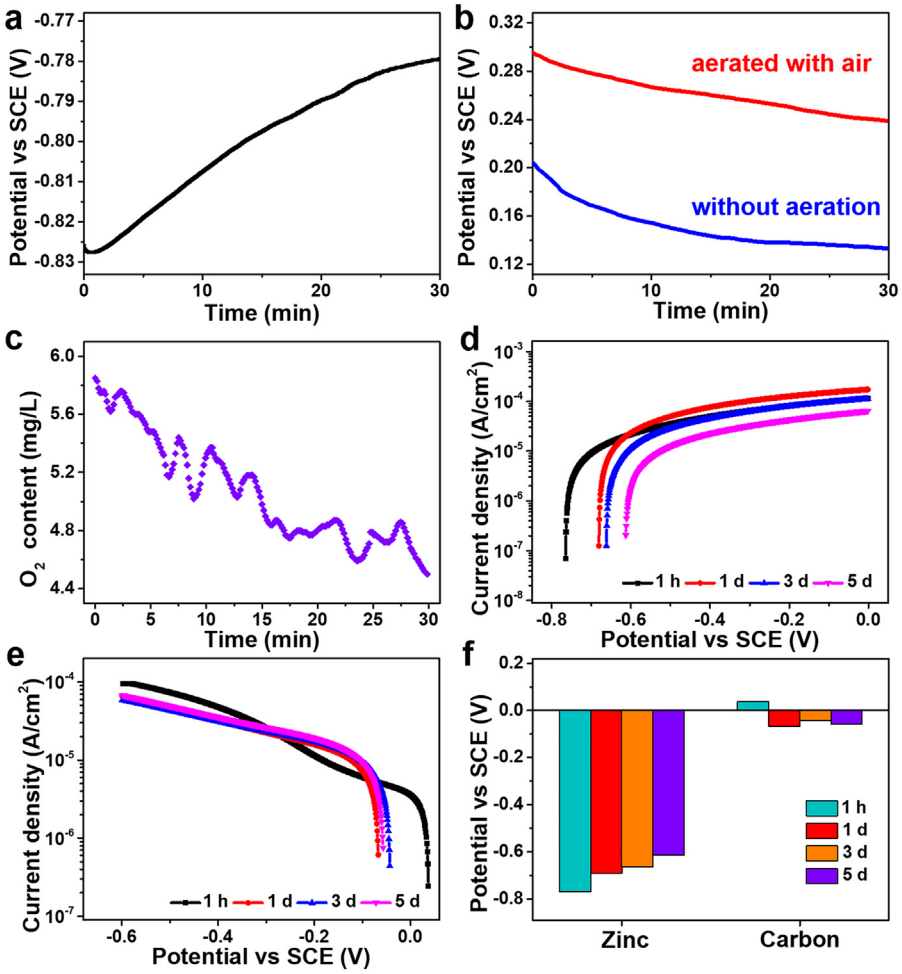

Fig. 4. (a) OCP of Zn sheet immersed in Cd^{2+} solution in 30 min; (b) OCP of C rod immersed in Cd^{2+} solution aerated with air for 15 min and without aeration in 30 min; (c) variation of O_2 content in Cd^{2+} solution treated with primary battery; (d) anodic polarization curves for Zn sheet; (e) cathodic polarization curves for C rod, and (f) OCP variation of Zn sheet and C rod in Cd^{2+} solution at 1 h, 1 d, 3 d and 5 d respectively.

mation of $Cd(OH)_2$ and ZnO (reactions (4) and (5)) and the consumption of dissolved O_2. As shown in Fig. 4b, the OCP of C in solution with 15-min aeration of air increases globally. Simultaneously, the dissolved O_2 in the electrolyte shows obvious consumption, whose content decreases from 5.85 to 4.50 mg/L (Fig. 4c) in a fluctuating way as the galvanic reactions in the primary battery continue. It is likely that its supply, such as dissolution in solution and diffusion toward the cathode, cannot meet the demand of free electrons at the cathode to generate OH^- (reaction (3)). Initially, we can confirm the passivation and consumption of O_2 in Cd^{2+} solution at the C cathode, and the supply of O_2 toward C seems to be the rate-determining step of O_2 reduction.

The anodic polarization curves for the Zn sheet and the cathodic polarization curves for the C rod in Cd^{2+} solution at different times were measured, as displayed in Fig. 4d and 4e, respectively. The curves for Zn comprise two regions of active and gradual dissolution at any time (1 h, 1 d, 3 d and 5 d). In the active dissolution process, Zn dissolves rapidly as the current density increases fast because a less passivation layer is formed. While the current density continues to increase gradually, even Zn is covered with a more passivation layer, indicating sustained reactions at the Zn anode. This also proves that the formed passivation layer is not compact enough to completely prevent galvanic reactions and is thus deemed a pseudopassive layer [32]. The layer shows some constraints on reactions at the anode, because the current density possesses the lowest value at 5 d (Fig. 4d) and the OCP of Zn keeps shifting to the anodic direction over time (Fig. 4f). In addition, the increase in current density at 1 d and 3 d may results from the enhancement of the conductivity of the solution with more dissolved ions. Similarly, the cathodic polarization curves (Fig. 4e) consist of active and gradual regions, having a porous passive layer to let the ions pass through. In gradual regions, the current density at a higher cathodic potential decreases, and the OCP of Zn shifts toward the cathodic direction with time, controlled by the O_2 supply and passive processes.

EIS diagrams were recorded with AC frequencies from 100 kHz to 10 mHz at OCPs for different times. Fig. S5 shows the Nyquist impedance plots obtained from Zn between 100 kHz and 1 kHz, and Fig. 5 displays the Nyquist impedance plots from 10 kHz to 10 mHz under immersion in Cd^{2+} solution for 1 h, 1 d, 3 d and 5 d. All the EIS spectra of Zn with higher frequency (Fig. S5) have less pronounced capacitive loops, which correspond to the stray capacitances related to the parameters of the primary battery instead of galvanic reactions [32]. The generation of capacitive loops over 10 kHz may be attributed to the high resistivity of the electrolyte with a low Cd^{2+} content of 100 mg/L, which exists in the actual polluted medium.

The impedance data at 1 h in Fig. 5a indicates merely one capacitive loop at high frequencies followed by a poorly defined inductive loop. The model (A) $\{R_s(Q_1(R_1(Q_2R_2)(LR)))\}$ [37] in Fig. 5b is applied to obtain a satisfactory fit to the EIS spectra. In the model, the constant phase elements (CPEs) Q_1 and Q_2 with parameter values (n) from 0 to 1 take the place of pure capacitance ($n = 1$), which can be affected by the complexity of the space charge layer and the surface properties of

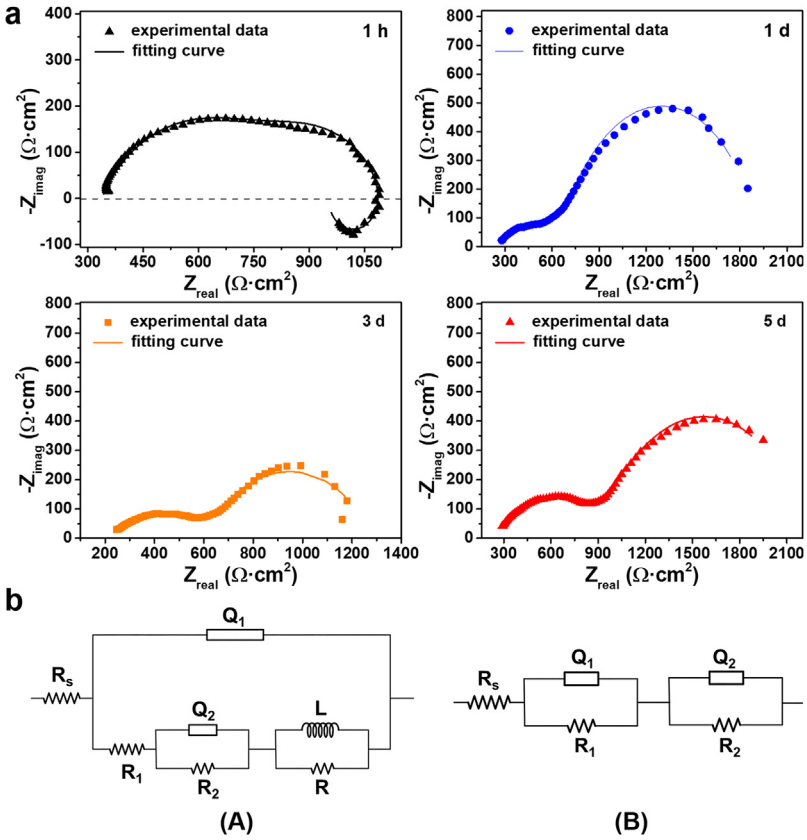

Fig. 5. (a) Nyquist plot and modeling of EIS spectra of Zn sheet immersed in Cd^{2+} aqueous solution for 1 h, 1 d, 3 d and 5 d respectively with frequency range from 10 kHz to 10 mHz; (b) equivalent circuits used to fit the EIS diagrams (Nyquist plot for 1 h fits with circuit model (A), the rest fit with circuit model (B)).

the Zn anode [32]. The R_1-Q_1 parallel network on the left of model (A) can be attributed to the faradic charge transfer process, while the R_2-Q_2 network may be relevant to the diffusion process. Table S1 shows the numerical data of the components in model (A). A large internal resistance (R_s) and relatively small charge transfer resistance (R_1) were recorded, which implies a low ion concentration in the electrolyte and an active reaction rate with less oxidation of Zn for the first time. According to the high C_2 value and relatively low R_2 value for Zn at 1 h, the passive layer on Zn is demonstrated to be porous. The inductance with a value of 580.4 H works at very low frequency and reflects the surface properties of Zn, such as adsorption and pitting corrosion.

Electrochemical impedance spectroscopy (EIS) spectra of Zn in Cd^{2+} solution at 1 d, 3 d and 5 d consist of two well-pronounced capacitive loops, as shown in Fig. 5a, which exhibit a satisfactory match with simulated curves based on model (B) {$R_s(Q_1R_1)(Q_2R_2)$} [32] in Fig. 5b. The first loop at high frequency (R_1-Q_1) corresponds to the charge transfer process, and the latter (R_2-Q_2) is related to the adsorption process to form a passive layer. The values of the components in model (B) are displayed in Table S1. In comparison to the EIS spectra at 1 h, R_s decreases with time, indicating that more dissolved ions are generated via galvanic reactions. In addition, the reaction rate of Zn can be evaluated by calculating the polarization resistance R_p, which equals the sum of R_1 and R_2. From 1 h to 5 d, R_p shows a fluctuating increase, implying a weakening of the reaction activity owing to the formation of a passive layer in Zn and C. As a result, the gradient of the Cd^{2+} RE curve (Fig. 2g) displays a sustained reduction. In addition, the value of n_1 in the EIS spectra, especially for 3 d and 5 d, approaches 0.5, suggesting the diffusion process across the passive layer. The capability of diffusion of active species helps to maintain the relatively active galvanic reactions to obtain continuous Cd^{2+} precipitation for a long time.

3.4. *Effect of the primary battery on water spinach and zebrafish in water*

A pot experiment was conducted to study the effect of CWBPB on water spinach, a widely consumed vegetable in Southeast Asia [38]. Cd^{2+} in water could pose an adverse impact on the growth of water spinach because Cd^{2+} uptake and accumulation induced the generation of toxic substances harmful to metabolism [39]. Fig. 6a-e show that water spinach could grow well in tap water and possess high plant height, root length, and chlorophyll content. However, these three parameters significantly decreased in Cd^{2+}-aqueous solution, showing that Cd^{2+} negatively affected the growth of water spinach. When water spinach was planted in water treated by CWBPB for 1 d, these three parameters increased to a certain extent. Notably, after CWBPB treatment for 5 d, these parameters increased dramatically to tap-water levels.

Additionally, Fig. 6f shows that the Cd content of water spinach in Cd^{2+} -aqueous solution was significantly higher than that of water spinach in tap water, showing that water spinach had a high uptake of Cd^{2+}. After the Cd^{2+} -aqueous solution was treated with CWBPB, the Cd content in water spinach substantially decreased with treatment time. In other words, CWBPB could efficiently inhibit Cd^{2+} -uptake by water spinach, which was attributed to the high removal ability of CWBPB on Cd^{2+}. These results indicated that CWBPB exhibited significant remediation ability against Cd^{2+} contamination and a positive effect on the growth of water spinach, which was beneficial to ensure food safety.

To further evaluate the remediation performance of CWBPB on Cd^{2+} in water, the effect of CWBPB on the growth of zebrafish was investigated, as it is a kind of model fish sensitive to Cd^{2+} [40]. It can be seen from Fig. 7a and 7b that all zebrafish lived normally in tap water within 24 h, while in Cd^{2+}-contaminated water, they floated to the top layer (above the yellow dashed line) after 6 h and died 24 h later.

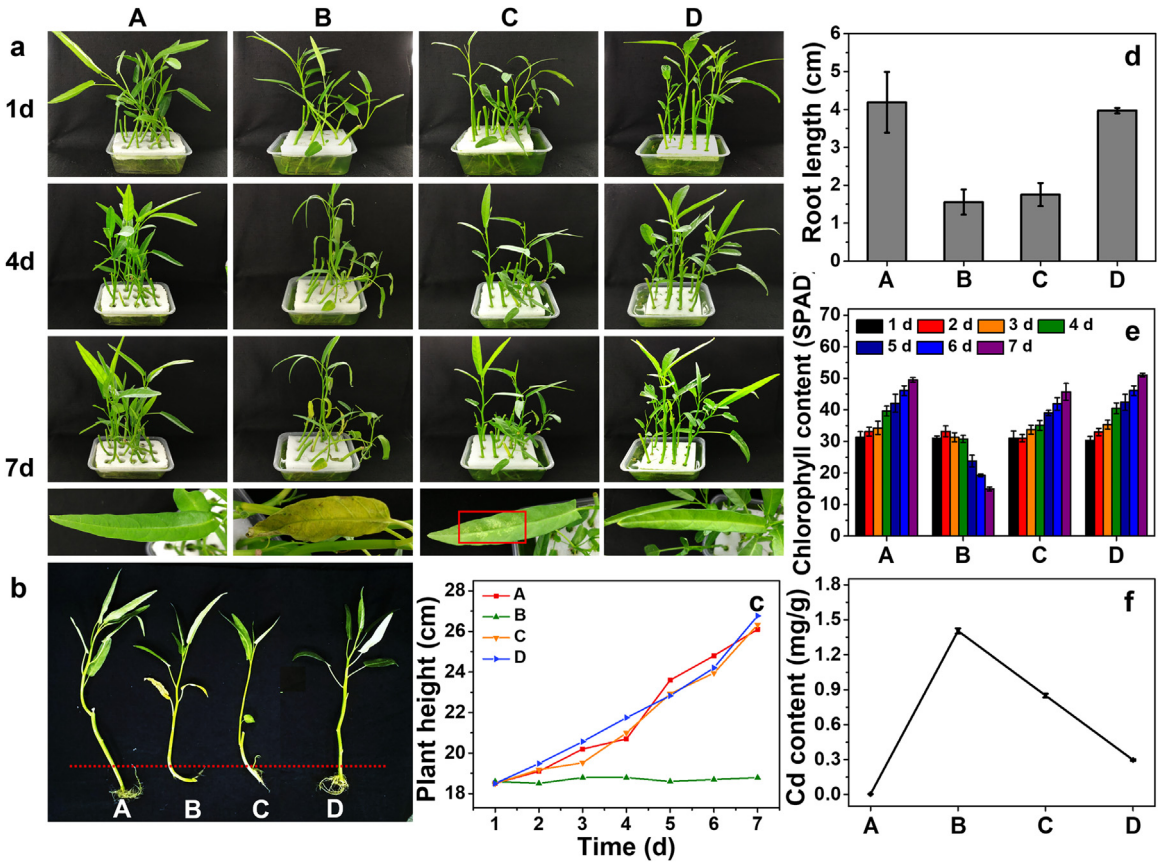

Fig. 6. (a and b) Digital images, (c) plant height, (d) root length, (e) chlorophyll content, and (f) Cd concentration of water spinaches in (A) 500 mL of tap water and (B-D) mixture of 450 mL of tap water and 50 mL of Cd^{2+} -aqueous solution after treatment with CWBPB (C_0 = 50 mg/L, 20 °C, pH = 6.5, tank size of 80 mm × 50 mm × 80 mm, electrode spacing of 6 cm and C rod diameter of 14 mm) for 0, 1 and 5 d respectively. The marked rectangle region in (a) shows the yellow spots on the leaf.

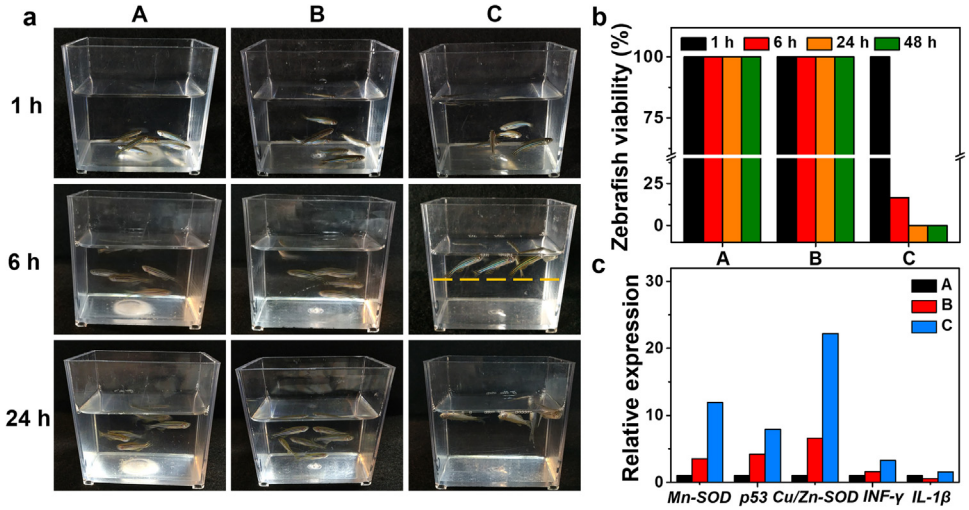

Fig. 7. (a) Digital images, (b) viability, and (c) gene expression of zebrafish in (A) 200 mL of tap water and (B, C) Cd^{2+}- contaminated water treated by CWBPB (C_0 = 12 mg/L, 20 °C, pH = 6.5, tank size of 80 mm × 50 mm × 80 mm, electrode spacing of 6 cm, and C rod diameter of 14 mm) for 5 and 0 d.

This result proved that Cd^{2+} at a certain concentration had a severely harmful effect on zebrafish. In the water after CWBPB treatment for 5 d, all zebrafish were still alive after 48 h, suggesting that CWBPB could effectively inhibit the negative impact of Cd^{2+} on zebrafish.

The effect of CWBPB on the expression of five genes (antioxidant system-related genes *Mn-SOD* and *Cu/Zn-SOD*, apoptosis-related gene *p53*, immune system-related genes *INF-γ* and *IL-1β*) in zebrafish was investigated. The expression levels of these genes, analyzed by qRT–PCR with the primers listed in Table S2, may be used to evaluate the extent of exposure to Cd^{2+} ions [41–43]. Fig. 7c shows that exposure to Cd^{2+}-contaminated water could cause significant upregulation of the expression of all these genes compared with tap water, demonstrating that Cd^{2+} exposure could induce oxidative stress, apoptosis, and immunotoxicity in zebrafish. After treatment with CWBPB for 5 d, the Cd^{2+} concen-

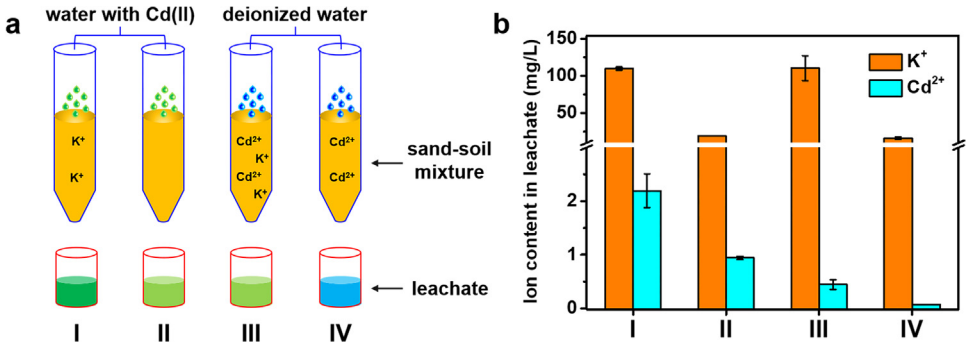

Fig. 8. (a) Schematic diagrams of different leaching systems: addition of Cd(II)-contaminated water on (I) soil-sand mixture containing K^+, and (II) pristine soil-sand mixture, addition of deionized water on (III) soil-sand mixture containing Cd^{2+} and K^+, and (IV) soil-sand mixture containing Cd^{2+} (6 mg); (b) Content of K^+ and Cd^{2+} in leachate of I, II, III and IV after leaching.

tration in water greatly decreased, and the gene expression of zebrafish was downregulated to a normal level. All animal experiments were approved by the Research Institute Ethics Committee of Hefei Institutes of Physical Science and were conducted according to the guidelines on the use and care of laboratory animals at Hefei Institutes of Physical Science.

3.5. Removal performance of the primary battery for Cd in soil

Generally, Cd in soil exists as soluble (Cd^{2+}) and insoluble ($Cd(OH)_2$, $CdCO_3$ etc.) forms, wherein the latter could be transformed to the former under certain conditions [44–46]. To substantially remediate Cd^{2+}-contaminated soil, the RE of CSBPB on total Cd was examined herein. Notably, the concept of CSBPB on efficient total Cd removal is to drive soluble Cd^{2+} aggregate together to precipitate followed by collection methods. Nevertheless, Cd^{2+} tends to be adsorbed via the negatively charged soil colloidal particles, resulting in a poor migration rate. As shown in Fig. 8, pristine soil–sand mixtures are capable of maintaining most Cd^{2+} after the addition of water containing Cd^{2+}, and the Cd^{2+}-included soil–sand keeps Cd^{2+} in after the addition of deionized water. Both mixtures display a significant increase in Cd^{2+} in leachates after the addition of K^+, also showing a higher K^+ content (I and III in Fig. 8). These results indicate that more K^+ in soil may contribute to the desorption of Cd^{2+} from soil colloidal particles through ion exchange, benefitting the migration of Cd^{2+} under an electric field.

According to the potential favorable effect of K^+ on the RE of the total Cd, the removal performances of the primary battery with KCl addition under different conditions were studied. As shown in Fig. 9a, at a Cd^{2+} addition amount of 15 mg, CSBPB could remove approximately 84% of total Cd in the middle part between the two electrodes within 120 h, and the RE decreased with increasing Cd^{2+} addition amount. Fig. 9b shows that the RE of total Cd increased significantly from 18.4% to 84% with the KCl addition amount. This was because the desorption of Cd^{2+} from soil particles via ion exchange, as illustrated above, improved soil conductivity to facilitate the galvanic reactions and migration of Cd^{2+} to the C rod. Therefore, the addition of K^+ resulted in the generation of a higher current (Fig. S6a) and more precipitates (Fig. S6b, c). Importantly, the added KCl could enhance soil fertility, favoring the growth of crops [33].

Additionally, the influence of C rod diameter and soil moisture on total Cd removal was investigated. As illustrated in Fig. 9c, with increasing C rod diameter, the RE increased because C rods with larger sizes possessed better conductivity to promote Cd^{2+} migration to the C rod and galvanic reactions. Similarly, the RE increased with increasing soil moisture (Fig. 9d) because higher moisture could favor the dissolution of ions in soil and soil conductivity. Fig. 9e shows that RE decreased gradually with increasing pH because lower pH could inhibit the formation of $Cd(OH)_2$ in soil and promote Cd^{2+} migration toward the cathode. Meanwhile, temperature displayed a positive effect on total Cd removal, as shown in Fig. 9f.

The RE of total Cd in Cd^{2+}-contaminated soil treated with CSBPB over time was investigated. As shown in Fig. 9g, RE increased rapidly from 0 to 82.6% during the initial 72 h and slowly from 82.6% to 84% during the next 48 h, which we attribute to the decrease in cathode conductivity with increasing precipitate amount on the C rod surface. Notably, Cd^{2+} RE even reached 99.2% (Fig. 9h), implying that most Cd^{2+} in the middle of the soil electrolyte migrated to the C rod and that the residual Cd^{2+} was transformed to $Cd(OH)_2$. For the sake of convenience and efficiency, a Zn sheet with a size of 60 × 35 × 2 mm^3 and a C rod with a diameter of 14 mm and length of 60 mm were chosen as the optimum conditions for the preparation of CWBPB and CSBPB. The corresponding estimated cost can be as low as approximately 0.11 USD/L and 0.79 USD/m^2. Details are provided in the supplementary materials (Table S3).

To obtain the components of the precipitates on the C rod surface after Cd removal by treatment, XRD measurements were performed. Fig. 9i shows that characteristic peaks of $Cd(OH)_2$ (18.9° (001), 29.5° (100), and 49.0° (102)) and ZnO (36.3° (101), 47.5° (102), and 56.6° (110)) were found in the XRD spectrum of the precipitates. This result indicated that the precipitates consisted of mainly $Cd(OH)_2$ and ZnO, which was consistent with that in water.

To further study the chemical states of the precipitates, XPS analyses were performed. As shown in Fig. 9j, the asymmetric O 1s peak could be deconvoluted into two peaks (531.6 and 532.5 eV), attributed to ZnO and $Cd(OH)_2$, respectively. In addition, Fig. 9k shows that the Zn $2p_{3/2}$ peak at 1022.3 eV attributed to ZnO also proved the existence of ZnO in the precipitates. Additionally, the Cd $3d_{3/2}$ and $3d_{5/2}$ peaks at 405.3 and 412.2 eV in Fig. 9l confirmed the existence of $Cd(OH)_2$ in the precipitates. The spectra of O 1s, Zn 2p, and Cd 3d agreed well with those of ZnO and $Cd(OH)_2$ in the NIST XPS database. Notably, the peaks of O 1s herein were slightly different from those in water, which can probably be attributed to the different environments in soil and water. These results demonstrated that the precipitates on the C rod in soil comprised the same compounds ($Cd(OH)_2$ and ZnO) as in water, which might be the reason for Cd removal by CSBPB.

3.6. Effect of the primary battery on Nicotiana benthamiana and Arabidopsis in soil

Nicotiana benthamiana (*N. benthamiana*) and *Arabidopsis*, two widely used model plants [47,48], were chosen to further evaluate the removal performance of CSBPB on Cd in soil. As shown in Fig. 10a and d, the *N. benthamiana* in Cd^{2+}-contaminated soil possessed significantly lower plant height and biomass compared with normal soil. After CSBPB treatment for 5 d, the two parameters increased substantially. Fig. 10c shows that the Cd amount of *N. benthamiana* in Cd^{2+}-contaminated soil was higher than that in normal soil, while it decreased dramatically after

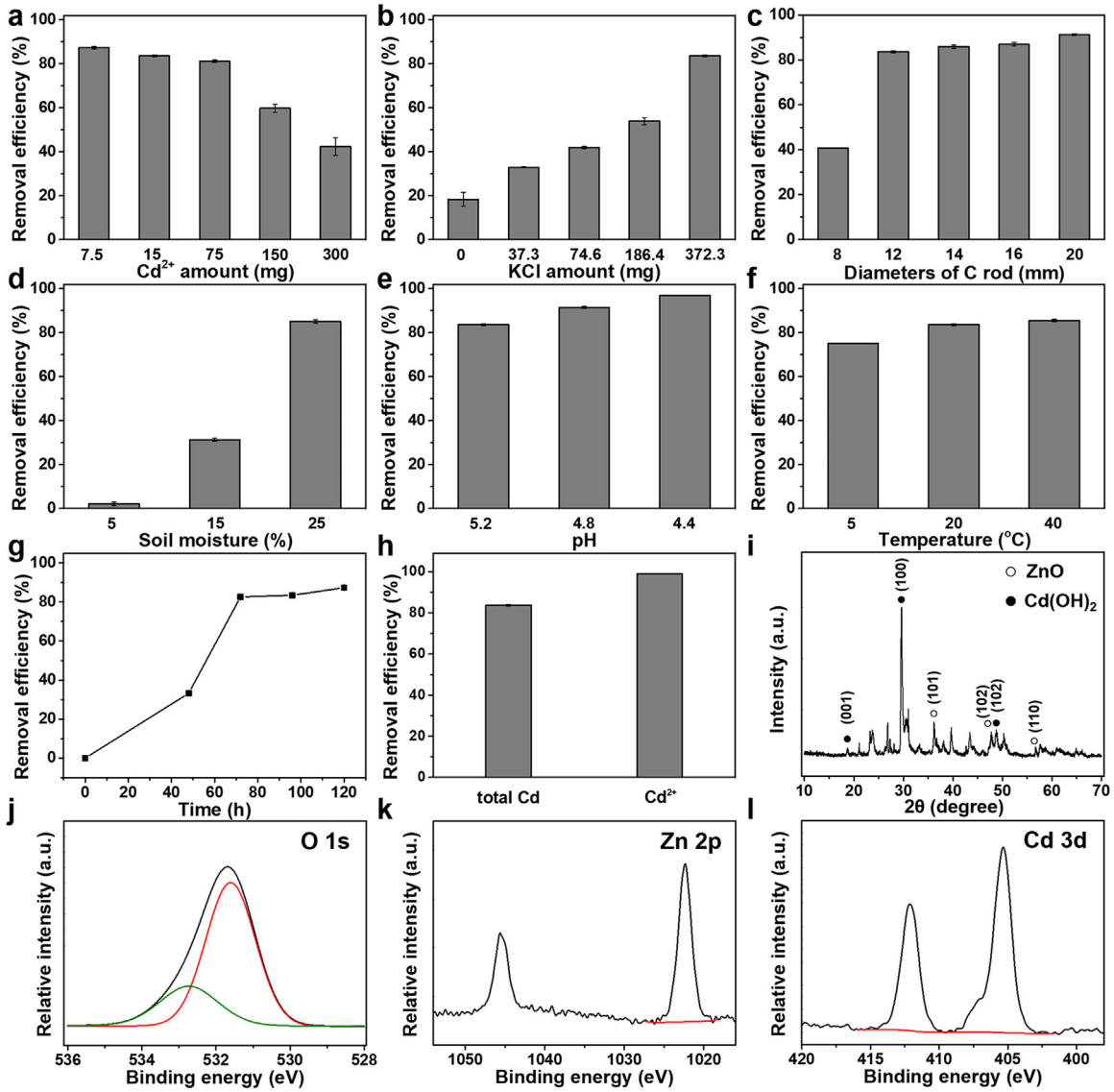

Fig. 9. Effects of (a) Cd^{2+} amount on RE of Cd (moisture of 25%, pH = 5.2, 20 °C, KCl amount of 372.8 mg, C rod diameter of 14 mm), (b) KCl amount on RE of Cd (moisture of 25%, pH = 5.2, 20 °C, Cd^{2+} amount of 15 mg, C rod diameter of 14 mm), (c) C rod diameter on RE of Cd (moisture of 25%, pH = 5.2, 20 °C, Cd^{2+} amount of 15 mg, KCl amount of 372.8 mg), (d) soil moisture on RE of Cd (pH = 5.2, 20 °C, Cd^{2+} amount of 15 mg, KCl amount of 372.8 mg, C rod diameter of 14 mm), (e) pH on RE of Cd (moisture of 25%, 20 °C, Cd^{2+} amount of 15 mg, KCl amount of 372.8 mg, C rod diameter of 14 mm), (f) temperature on RE of Cd (moisture of 25%, pH = 5.2, Cd^{2+} amount of 15 mg, KCl amount of 372.8 mg, C rod diameter of 14 mm) from Cd^{2+}-contaminated soil by CSBPB (tank size of 80 × 50 × 80 mm^3, electrode spacing of 4 cm) for 5 d; (g) RE of total Cd with time and (h) RE of total Cd and Cd^{2+} (for 120 h) from Cd^{2+}-contaminated soil by CSBPB (moisture of 25%, pH = 5.2, 20 °C, Cd^{2+} amount of 7.5 mg, KCl amount of 372.8 mg, C rod diameter of 14 mm); (i) XRD and XPS spectra (j-l: O 1s, Zn 2p, Cd 3d) of precipitates on C rod surface after CSBPB treatment.

5 d of CSBPB treatment. These results indicated that CSBPB could efficiently promote the growth of *N. benthamiana* and reduce Cd uptake. Similar results were found in the pot experiment of *Arabidopsis*, as shown in Figs. 10b, 10e, and 10f. Notably, *Arabidopsis* blossomed earlier (white arrow in Fig. 10b) under Cd^{2+} stress in Cd^{2+}-contaminated soil than in normal and CSBPB-treated Cd^{2+}-contaminated soil. These results suggested that CSBPB treatment had significantly positive effects on the growth of *N. benthamiana* and *Arabidopsis* and their Cd uptake because CSBPB could effectively remove Cd from Cd^{2+}-contaminated soil.

3.7. Bacterial community structure analysis of soil

The influence of CSBPB treatment on the bacterial community structure in soil was investigated through 16S rRNA gene fragment pyrosequencing. The species richness of the bacteria was assessed with the operational taxonomic unit (OTU) number and Chao and ACE indices. As shown in Table S4, Cd^{2+}-contaminated soil exhibited a greater OTU number and Chao and ACE indices than normal soil, indicating that Cd^{2+} stress could improve species richness. After CSBPB treatment, Cd^{2+}-contaminated soil possessed almost the same species richness as normal soil, implying that CSBPB could effectively decrease the amount of Cd. Furthermore, Cd^{2+}-contaminated soil possessed a higher Shannon index and lower Simpson index than normal soil, suggesting that Cd^{2+} stress could cause higher bacterial diversity. When the Cd^{2+}-contaminated soil was treated with CSBPB, the bacterial diversity decreased, suggesting the good remediation performance of CSBPB on Cd^{2+}-contaminated soil.

In addition, differences in bacterial community structure between normal soil and Cd^{2+}-contaminated soil were found in the taxonomic analysis. As shown in Fig. 11a, the highest richness of the bacterial phylum in normal soil was Firmicutes (70.42%), followed by Proteobacteria (14.26%), Actinobacteria (10.09%), Acidobacteria (1.57%), Gemmatimonadetes (1.07%), and Bacteroidetes (0.74%). Therein, the total relative abundance of gram-positive bacteria (Firmicutes and Actinobacteria) was 80.51%, and that of gram-negative bacteria (Pro-

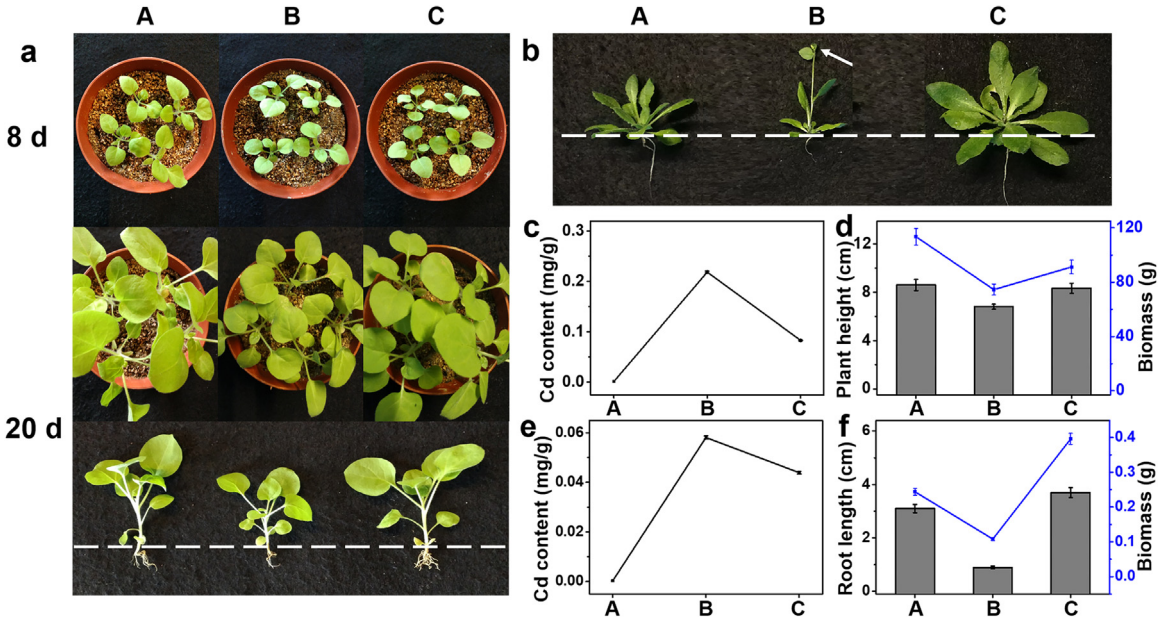

Fig. 10. Digital photos of (a) *N. benthamiana* and (b) *Arabidopsis* in (A) normal soil and (B, C) Cd^{2+}-contaminated soil treated by CSBPB for 0 and 5 d; (c, d) Cd concentration, plant height, and biomass of *N. benthamiana*; (e, f) Cd concentration, root length, and biomass of *Arabidopsis*.

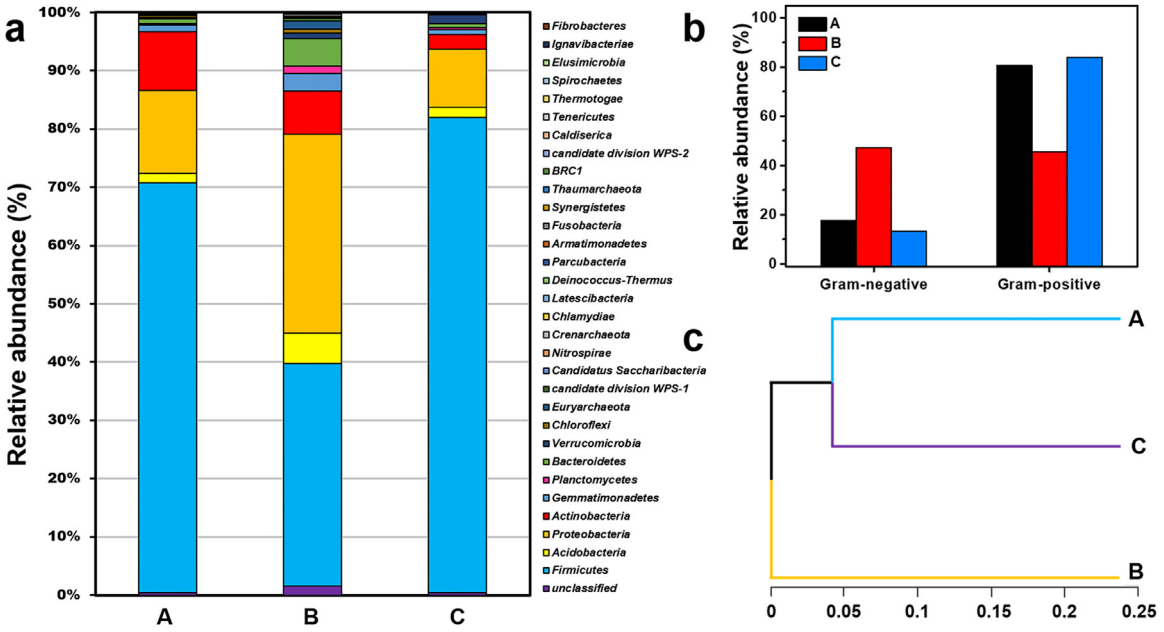

Fig. 11. Relative abundance at the phylum level of (a) bacteria, (b) Gram-negative and Gram-positive bacteria, and (c) cluster diagram of (A) normal soil and (B, C) Cd^{2+} (C_0 = 37.5 mg/kg)-contaminated soil after treatment with CSBPB-contaminated soil after treatment with CSBPB (moisture of 25%, pH = 5.2, 20 °C, KCl amount of 372.8 mg, tank size of 80 mm × 50 mm × 80 mm, C rod diameter of 14 mm, electrode spacing of 4 cm) for 0 and 5 d.

teobacteria, Acidobacteria, Gemmatimonadetes, Bacteroidetes) reached only 17.63%. Nevertheless, gram-positive bacteria, including Firmicutes (38.17%) and Actinobacteria (7.41%), were less abundant in soil containing Cd (Fig. 11b), in contrast to the relative abundance of gram-negative bacteria, which all displayed significant increases, and their total abundance increased to 47.12%. This result indicated that the species of Proteobacteria, Acidobacteria, Gemmatimonadetes, and Bacteroidetes may resist Cd toxicity. After CSBPB treatment, their relative abundances returned to normal soil levels (84.06% for gram-positive bacteria and 13.2% for gram-negative bacteria).

In addition, the cluster diagram of bacteria was calculated through Bray-Curtis dissimilarity (97% OTU cluster). The cluster analysis results in Fig. 11c show that the bacterial community in Cd^{2+}-contaminated soil was different from that in normal soil. After CSBPB treatment, Cd^{2+}-contaminated soil had a similar bacterial community to normal soil. These results proved that CSBPB could efficiently remove Cd from soil and inhibit its negative effect on soil bacterial community structure.

3.8. Electricity generation of the primary battery

The influence of CSBPB on the distributions of Cd, Cd RE, Zn, and pH between the anode and cathode in Cd^{2+}-contaminated soil was investigated through the system in Fig. 12a. As shown in Fig. 12b, Cd was distributed evenly at first. After CSBPB treatment for a given time, the

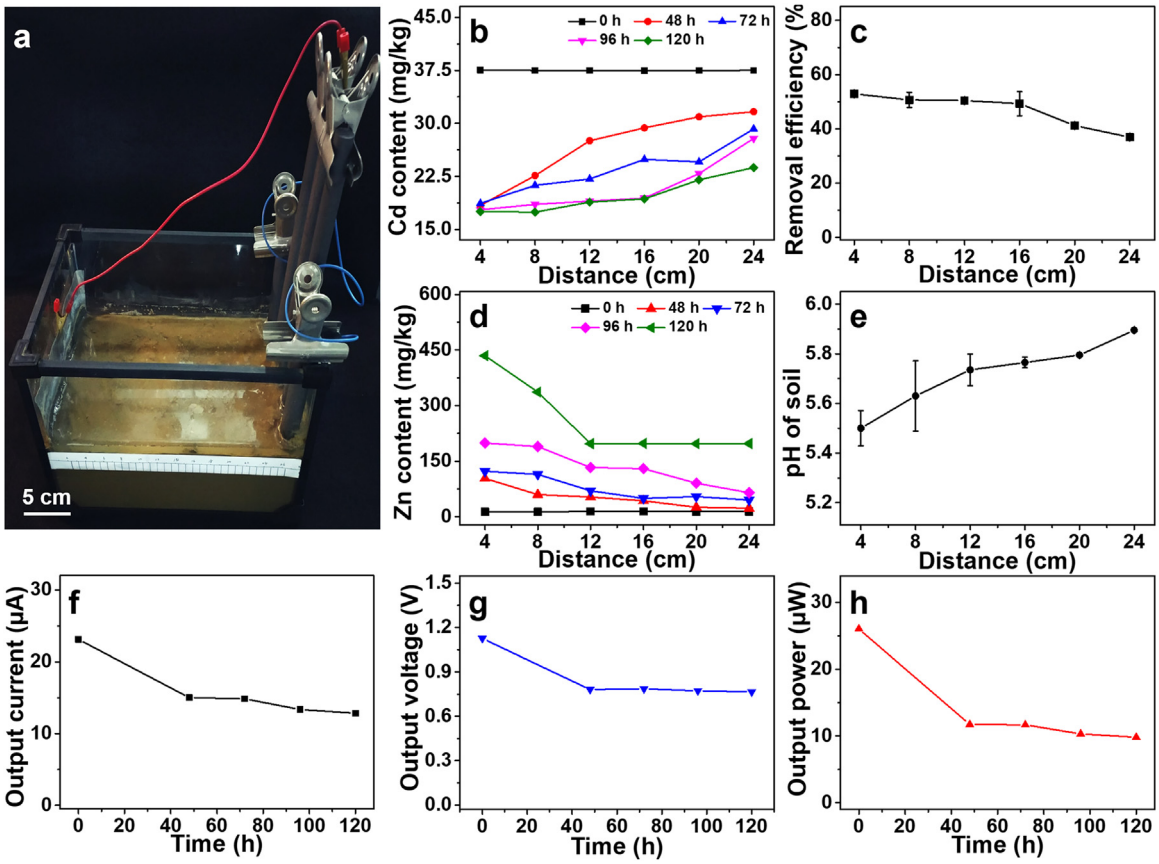

Fig. 12. (a) Digital image of a CSBPB (Cd^{2+} amount of 350 mg, moisture of 25%, pH = 5.2, 20 °C, KCl amount of 18.64 g, five C rods with diameter of 20 mm each, electrode spacing of 28 cm) with 9.33 kg of Cd^{2+}-contaminated soil in a tank (300 mm × 180 mm × 200 mm); (b) Cd content, (c) RE of Cd after 120 h, (d) Zn content, and (e) pH of Cd^{2+}-contaminated soil after 120 h with different distances from anode; (f-h) output current, voltage, and power of this CSBPB.

Cd content increased with the distance from the anode, implying Cd^{2+}-migration from the anode to the cathode and accumulation around the C rod under an electric field. At any distance, the Cd content decreased with time, suggesting that Cd^{2+} migrated gradually to the cathode and that some of it was then adsorbed by the C rod. After 120 h, such Cd^{2+} migration resulted in the Cd RE decreasing from 52.9% to 36.9% with distances from 4 to 24 cm to the anode (Fig. 12c).

As displayed in Fig. 12d, little Zn was found in the soil between the two electrodes at first. After CSBPB treatment, the Zn content increased with time at a certain distance, while at a certain time, it decreased with distance, exhibiting a contrasting trend to that of Cd. This result proved the occurrence of reaction (1) around the anode to generate a certain amount of Zn^{2+}, which partially migrated toward the cathode under an electrical field. Additionally, the electrons of Zn could migrate to the C rod via copper wire, resulting in the occurrence of reaction (3) around the cathode to produce OH^-, which partially migrated toward the anode under an electrical field. As shown in Fig. 12e, the pH of the soil slowly increased from 5.5 to 5.9 with distance from the anode after 120 h, implying that the pH was relatively stable. This was likely because most OH^- had reacted with Cd^{2+} or Zn^{2+}. The relatively stable pH was good for the environment.

Attributed to the spontaneous redox reactions (1–3) within Cd^{2+}-contaminated soil, chemical energy was transformed to electrical energy, generating electricity in the circuit. As shown in Figs. 12f, 12g and 12h, the output current, voltage, and power of CSBPB reached 23 μA, 1.13 V, and 26.0 μW initially, decreased to 16 μA, 0.78 V, and 12 μW after 44 h, and then these values decreased rather slowly from 44 to 120 h. This result indicated that CSBPB efficiently generated electricity that could last for more than 120 h.

To obtain relatively high electricity, four primary batteries based on Cd^{2+}-contaminated water and soil were connected in series (Fig. 13a and 13b). They could generate output powers of 726 and 908 μW, respectively, and power LED lights (as shown in Fig. 13a-f and supplementary video). After 10 d, their powers decreased to 197 and 837 μW, respectively, and the intensities of LEDs decreased correspondingly, implying that their powers could last for at least 10 d. Therein, the soil-based LED possessed a higher stability than the water-based LED because Cd^{2+} and Zn^{2+} had relatively low migration performance in soil compared with water. These results demonstrated that the primary batteries based on both Cd^{2+}-contaminated water and soil could generate relatively high electricity. Importantly, the electricity could be conveniently adjusted through the number of connected primary batteries in series, which was beneficial for the application.

3.9. Empirical models of output current and Re

To predict the output current and Cd^{2+} RE of CWBPB in water under different conditions, two empirical models (Eqs. 6 and 7) were established through nonlinear fitting according to the experimental results in Table S5,

$$\ln I = 0.425 \ln C_0 - 0.0417 \ln d - 0.124 t^{0.502} + 4.696 \quad (6)$$

$$RE = \left[t^{1.113} \exp(-0.845 t^{0.297})\right] / \left(d^{0.425} C_0^{0.313}\right) \quad (7)$$

where C_0 is the Cd^{2+} initial concentration, I is electricity, d is the electrode spacing, and t is time. Fig. 14 shows that the theoretical data of these two models fit well with the experimental data. According to model (1), the electricity showed a positive correlation with Cd^{2+} initial concentration and negative correlations with electrode spacing and time. According to model (2), Cd^{2+} RE had a positive correlation with time and a negative correlation with Cd^{2+} initial concentration and electrode spacing, which was consistent with the preceding results in Fig. 2.

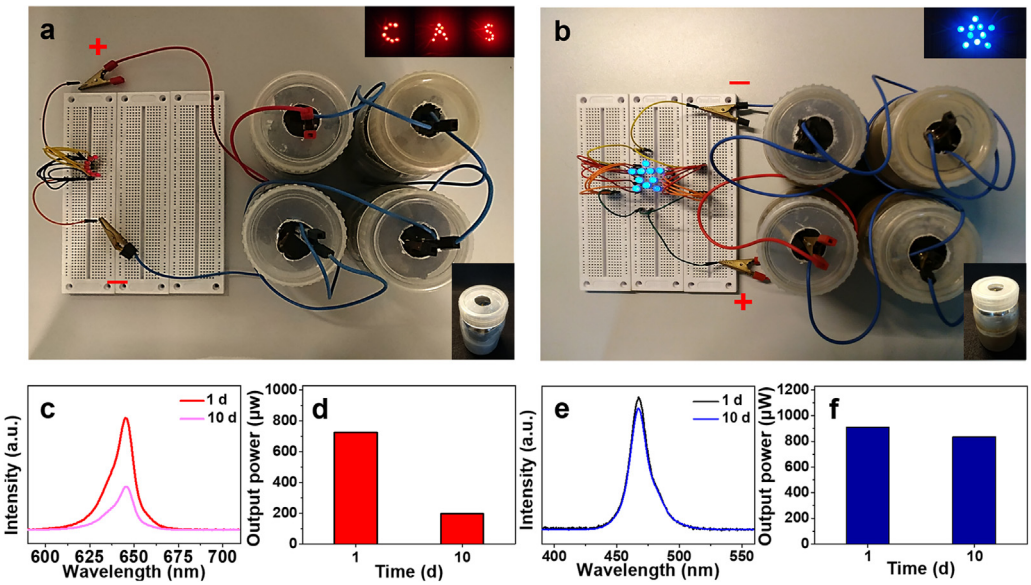

Fig. 13. Digital images of series circuits with four primary batteries based on Cd^{2+}-contaminated (a) water and (b) soil (upper right corner: alight LEDs; bottom right corner: water- or soil-based primary battery); (c, e) emission spectra of red and blue LEDs; (f) output powers of water-based and soil-based primary batteries.

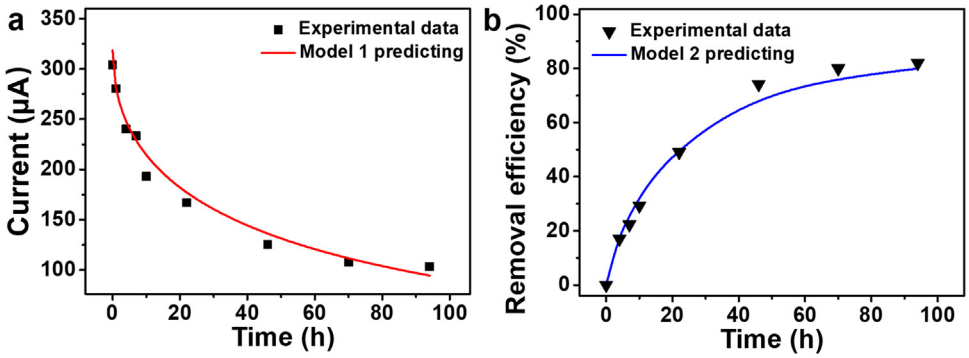

Fig. 14. Experimental data and predictive curves of (a) current (model 1) and (b) Cd^{2+} RE (model 2) of a CWBPB (C_0 = 100 mg/L, d = 4 cm, 20 °C, pH = 6.5, tank size of 80 × 50 × 80 mm^3 and C rod diameter of 14 mm).

4. Conclusion

Herein, to remove Cd^{2+} in water and soil, CWBPB and CSBPB consisting of a Zn anode, carbon (C) cathode, electrolyte (Cd^{2+}-contaminated water or soil), and copper wire were constructed. Therein, redox reactions occurred spontaneously, making electrons migrate efficiently from the anode to cathode, resulting in Zn^{2+} around the anode, OH^- around the cathode, and an electric field between these two electrodes. Subsequently, Cd^{2+} ions between these two electrodes, driven by electric field force, move toward the cathode and react with OH^- to obtain $Cd(OH)_2$ precipitate, exhibiting excellent removal of Cd^{2+}. According to the electrochemical investigation, the removal of Cd^{2+} proved to be sustainable for a long time even if the two electrodes were passivated. This technology could effectively promote the growth of plants and zebrafish, reduce their Cd uptake, and facilitate the soil bacterial community. Notably, this system could transform chemical energy to electrical energy and generate output powers of 725 and 908 μW in Cd^{2+} (800 mg/kg)-contaminated water and soil, respectively, being able to power LED lights for days. Additionally, two empirical models were built to predict the Cd^{2+} removal efficiency and output current under different conditions. This work provides a low-cost and environmentally friendly approach to remediate Cd^{2+} contamination and generate electricity simultaneously.

Author contributions

Chaowen Chen designed the overall research with Dongqing Cai, Jia Zhang and Zhengyan Wu providing guidance. Guilong Zhang designed and conducted electrical performance tests. Dongfang Wang performed the pot experiments. Jun Wang carried out the electrochemical measurements. Chaowen Chen conducted the empirical model simulation with Dongqing Cai providing guidance. Chaowen Chen, Dongqing Cai and Zhengyan Wu wrote the manuscript with input from all authors.

Data availability

The data that support the findings of this study are available from the corresponding authors upon reasonable request.

Declaration of competing interest

The authors declare that they have no conflicts of interest in this work.

Acknowledgments

The authors acknowledge the financial support from the Plan of Anhui Major Provincial Science and Technology Project

(202203a06020001), the University Synergy Innovation Program of Anhui Province (GXXT-2021–059), the National Natural Science Foundation of China (31771284, 52000025), the Key R&D Program of Guangdong Province (2020B0202010005), the Fundamental Research Funds for the Central Universities (2232020D-22), the Key R&D Program of Inner Mongolia Autonomous Region (2021GG0300), the Open Research Fund of Key Laboratory of Environmental Toxicology and Pollution Control Technology of Anhui Province and the Open Research Fund of Key Laboratory of High Magnetic Field and Ion Beam Physical Biology.

Supplementary materials

Supplementary material associated with this article can be found, in the online version, at doi:10.1016/j.fmre.2023.03.001.

References

[1] Y. Liu, J. Qiao, Y. Sun, X. Guan, Simultaneous sequestration of humic acid-complexed Pb(II), Zn(II), Cd(II), and As(V) by sulfidated zero-valent iron: Performance and stability of sequestration products, Environ. Sci. Technol. 56 (2022) 3127–3137.
[2] R. Li, X. Zhang, G. Wang, et al., Remediation of cadmium contaminated soil by composite spent mushroom substrate organic amendment under high nitrogen level, J. Hazard. Mater. 430 (2022) 128345.
[3] Y. Zong, Q. Xiao, S. Lu, Biochar derived from cadmium-contaminated rice straw at various pyrolysis temperatures: Cadmium immobilization mechanisms and environmental implication, Bioresour. Technol. 321 (2021) 124459.
[4] V. Gupta, A. Nayak, Cadmium removal and recovery from aqueous solutions by novel adsorbents prepared from orange peel and Fe_2O_3 nanoparticles, Chem. Eng. J. 180 (2012) 81–90.
[5] Z. Chen, X. Zhu, X. Lv, et al., Alleviative effects of C60 on the trophic transfer of cadmium along the food chain in aquatic environment, Environ. Sci. Technol. 53 (2019) 8381–8388.
[6] U. Garg, M. Kaur, G. Jawa, et al., Removal of cadmium (II) from aqueous solutions by adsorption on agricultural waste biomass, J. Hazard. Mater. 154 (2008) 1149–1157.
[7] Y. Su, A. Adeleye, Y. Huang, et al., Simultaneous removal of cadmium and nitrate in aqueous media by nanoscale zerovalent iron (nZVI) and Au doped nZVI particles, Water Res. 63 (2014) 102–111.
[8] P. Grimshaw, J. Calo, G. Hradil, Cyclic electrowinning/precipitation (CEP) system for the removal of heavy metal mixtures from aqueous solutions, Chem. Eng. J. 175 (2011) 103–109.
[9] H. Sakai, S. Matsuoka, A. Zinchenko, Removal of heavy metal ions from aqueous solutions by complexation with DNA and precipitation with cationic surfactant, Colloids Surf., A 347 (2009) 210–214.
[10] A. Khedr, Membrane methods in tailoring simpler, more efficient, and cost effective wastewater treatment alternatives, Desalination 222 (2008) 135–145.
[11] E. Pehlivan, T. Altun, Ion-exchange of Pb^{2+}, Cu^{2+}, Zn^{2+}, Cd^{2+}, and Ni^{2+} ions from aqueous solution by Lewatit CNP 80, J. Hazard. Mater. 140 (2007) 299–307.
[12] M. Iqbal, A. Saeed, S. Zafar, FTIR spectrophotometry, kinetics and adsorption isotherms modeling, ion exchange, and EDX analysis for understanding the mechanism of Cd^{2+} and Pb^{2+} removal by mango peel waste, J. Hazard. Mater. 164 (2009) 161–171.
[13] Z. Chen, Y. Liang, D. Jia, et al., Layered silicate rUB-15 for efficient removal of UO_2^{2+} and heavy metal ions by ion-exchange, Environ. Sci. Nano. 4 (2017) 1851–1858.
[14] U. Garg, M. Kaur, G. Jawa, Removal of cadmium (II) from aqueous solutions by adsorption on agricultural waste biomass, J. Hazard. Mater. 154 (2008) 1149–1157.
[15] Z. Li, T. Katsumi, S. Imaizumi, et al., Cd(II) adsorption on various adsorbents obtained from charred biomaterials, J. Hazard. Mater. 183 (2010) 410–420.
[16] Q. Zhu, Z. Li, Hydrogel-supported nanosized hydrous manganese dioxide: synthesis, characterization, and adsorption behavior study for Pb^{2+}, Cu^{2+}, Cd^{2+}, and Ni^{2+}, removal from water, Chem. Eng. J. 281 (2015) 69–80.
[17] J. Kheriji, D. Tabassi, B. Hamrouni, Removal of Cd(II) ions from aqueous solution and industrial effluent using reverse osmosis and nanofiltration membranes, Water Sci. Technol. 72 (2015) 1206–1216.
[18] A. Jakob, S. Stucki, P. Kuhn, Evaporation of heavy metals during the heat treatment of municipal solid waste incinerator fly ash, Environ. Sci. Technol. 29 (1995) 2429–2436.
[19] D. Kim, B. Ryu, S. Park, et al., Electrokinetic remediation of Zn and Ni-contaminated soil, J. Hazard. Mater. 165 (2009) 501–505.
[20] R. Probstein, R. Hicks, Removal of contaminants from soils by electric fields, Science 260 (1993) 498–503.
[21] B. Liu, S. Wang, P. Zhao, High-performance polyamide thin-film composite nanofiltration membrane: role of thermal treatment, Appl. Surf. Sci. 435 (2017) 415–423.
[22] E. Erdem, N. Karapinar, R. Donat, The removal of heavy metal cations by natural zeolites, J. Colloid Interface Sci. 280 (2004) 309–314.
[23] M. Shen, Y. Chen, H. Han, et al., Study on Electrokinetic remediation of Cadmium–contaminated soil, Agric. Biotechnol. 8 (2019) 139–143.
[24] A. Giannis, D. Pentari, J. Wang, et al., Application of sequential extraction analysis to electrokinetic remediation of cadmium, nickel and zinc from contaminated soils, J. Hazard. Mater. 184 (2010) 547–554.
[25] F. Cheng, J. Chen, X. Gou, et al., High-power alkaline Zn-MnO_2 batteries using γ-MnO_2 nanowires/nanotubes and electrolytic zinc powder, Adv. Mater. 17 (2010) 2753–2756.
[26] M. Winter, R. Brodd, What are batteries, fuel cells, and supercapacitors? Cheminform 104 (2004) 4245–4270.
[27] N. Zhang, F. Cheng, J. Liu, et al., Rechargeable aqueous zinc-manganese dioxide batteries with high energy and power densities, Nat. Commun. 8 (2017) 12267–12276.
[28] N. Xu, Y. Cai, L. Peng, et al., Superior stability of a bifunctional oxygen electrode for primary, rechargeable and flexible Zn-air batteries, Nanoscale 10 (2018) 13626–13637.
[29] E. Madej, M. Espig, R. Baumann, et al., Optimization of primary printed batteries based on Zn/MnO_2, J. Power Sources. 261 (2014) 356–362.
[30] J. Jindra, J. Mrha, M. Musilová, Zinc-air cell with neutral electrolyte, J. Appl. Electrochem. 3 (1973) 297–301.
[31] M. Mouanga, P. Berçot, J. Rauch, Comparison of corrosion behaviour of zinc in NaCl and in NaOH solutions. Part I: corrosion layer characterization, Corros. Sci. 52 (2010) 3984–3992.
[32] M. Mouanga, P. Berçot, Comparison of corrosion behaviour of zinc in NaCl and in NaOH solutions; Part II: electrochemical analyses, Corros. Sci. 52 (2010) 3993–4000.
[33] S. Khan, R. Mulvaney, Ellsworth, The potassium paradox: Implications for soil fertility, crop production and human health, Renew Agr. Food Syst. 29 (2014) 3–27.
[34] J. Zhou, J. Ao, Y. Xia, et al., Stable photoluminescent ZnO@$Cd(OH)_2$, core-shell nanoparticles synthesized via ultrasonication-assisted sol-gel method, J. Colloid Interface Sci. 393 (2013) 80–86.
[35] M Sandoval-Paz Rodríguez, G. Cabello, Characterization of ZnS thin films synthesized through a non-toxic precursors chemical bath, Mater. Res. Bull. 60 (2014) 313–321.
[36] N. Singh, S. Charan, K. Patil, et al., Unusual formation of nano-particles of CdO and $Cd(OH)_2$ from the reaction of dimethyl cadmium with DMF, Mater. Lett. 60 (2006) 3492–3498.
[37] S. Manov, A. Lamazouere, L. Aries, Electrochemical study of the corrosion behaviour of zinc treated with a new organic chelating inhibitor, Corros. Sci. 42 (2000) 1235–1248.
[38] R. Kumar, J. Chawla, Removal of cadmium ion from water/wastewater by nano-metal oxides: A review, Water Qual., Exposure Health 5 (2014) 215–226.
[39] D. Wang, G. Zhang, Z. Dai, et al., Sandwich-like nano-system for simultaneous removal of Cr(VI) and Cd(II) from water and soil, ACS Appl. Mater. Interfaces. 10 (2018) 18316–18326.
[40] K. Chan, L. Ku, P. Chan, et al., Metallothionein gene expression in zebrafish embryo-larvae and ZFL cell-line exposed to heavy metal ions, Mar. Environ. Res. 62 (2006) S83–S87.
[41] F. Fidalgo, R. Freitas, R. Ferreira, et al., Solanum nigrum L. Antioxidant defence system isozymes are regulated transcriptionally and posttranslationally in Cd-induced stress, Environ. Exp. Bot. 72 (2011) 312–319.
[42] A. Luzio, S. Monteiro, A. Fontaínhas-Fernandes, et al., Copper induced upregulation of apoptosis related genes in zebrafish (Danio rerio) gill, Aquat. Toxicol. 128 (2013) 183–189.
[43] A. Ray, A. Bhaduri, N. Srivastava, et al., Identification of novel signature genes attesting arsenic-induced immune alterations in adult zebrafish (Danio rerio), J. Hazard. Mater. 321 (2017) 121–131.
[44] Y. Ge, P. Murray, W. Hendershot, et al., Trace metal speciation and bioavailability in urban soils, Environ. Pollut. 107 (2000) 137–144.
[45] A. Ayoub, B. McGaw, C. Shand, et al., Phytoavailability of Cd and Zn in soil estimated by stable isotope exchange and chemical extraction, Plant Soil 252 (2003) 291–300.
[46] S. Iretskaya, S. Chien, R. Menon, Effect of acidulation of high cadmium containing phosphate rocks on cadmium uptake by upland rice, Plant Soil 201 (1998) 183–188.
[47] V. Nekrasov, B. Staskawicz, D. Weigel, et al., Targeted mutagenesis in the model plant Nicotiana Benthamiana using cas9 RNA-guided endonuclease, Nat. Biotechnol. 31 (2013) 691–693.
[48] M. Koornneef, D. Meinke, The development of Arabidopsis as a model plant, Plant J. 61 (2010) 909–921.

Chaowen Chen (BRID: 08665.00.72163) obtained his Ph.D. degree from the University of Science and Technology of China (USTC) in October 2020. Since November 2020, he has been a postdoctoral fellow in Hefei Institutes of Physical Science, China. His-research interests include the development and application of nanomaterials on environment and agriculture.

Zhengyan Wu (BRID: 09710.00.63818) obtained his Ph.D. degree from the Changchun Institute of Applied Chemistry in China in December 2000. From April 2001 to May 2002, he worked as a postdoctoral fellow in Université Louis Pasteur in France. From July 2002 to September 2008, he worked as a research associate in the Albert Einstein College of Medicine in USA. Since October 2008, he has been a professor in Hefei Institutes of Physical Science, China. His main work focuses on Environmental material and Biomaterial.